Gluing free assembly of an advanced 3D structure using visual servoing.

Sounkalo Dembélé, Nadine Le Fort-Piat, Naresh Marturi, Brahim Tamadazte

Gluing free assembly of an advanced 3D structure using visual servoing

Sounkalo Dembélé, Nadine Piat, Naresh Marturi and Brahim Tamadatze,
FEMTO-ST Institute, UMR CNRS 6174 - UFC / ENSMM / UTBM
Automatic Control and Micro-Mechatronic Systems Department
24, rue Alain Savary, 25000 Besançon, FRANCE
sounkalo.dembele@femto-st.fr

***Abstract*— The paper deals with robotic assembly of 5 parts by their U-grooves to achieve stables 3D MEMS, without any use of soldering effect. The parts and their grooves measure 400 μm $\times$ 400 μm $\times$ 100 μm $\pm$ 1.5 μm and 100 μm $\times$ 100 μm $\times$ 100 μm $\pm$ 1.5 μm leading to an assembly clearance ranging from -3 and +3 μm. Two visual servo approaches are used simultaneously: 2D visual servo for gripping and release of parts and 3D visual servo for displacement of parts. The results of experiments are presented and analyzed.**

Keywords: 3D microassembly, 3D MEMS, 2D visual servoing, 3D visual servoing

I. Introduction

Since many years CMOS and specially MEMS technologies enable manufacturing of 2D structures and devices that have to be assembled into 3D microsystems such as are 3D photonic chips ([1], [2], [3], [4]), [5], [6]), 3D electronic chips using Through Silicon Vias ([7], [8], [9], [10]), 3D fluidic chips ([11], [12]), ball bearing, laser diodes. They increase the number of functions per unit volume and provide new functionalities paving the way for original solutions to known problems as well as for new applications.
Robotic assembly is the main solution to these manipulations in the 3D space, the other being self-assembly. It involves multiple degree-of- freedom robotic and gripping systems in conjunction with multifocal imaging systems leading to the natural use of visual servoing approaches. These are precise and robust, and then fit particularly the requirements of microscale manipulations. Many work have investigated 3D assembly from this point-of-view:

- insertion of peg into hole ([13], [14], [15], [16], [17], [18], [19], [20], [21]),
- assembly of 3D devices ([22], [23], [24], [25], [26]), [27], [28],
- ball arrangement ([29]).

In these papers, the modeling of the sequence of motions is rarely performed. But it facilitates understanding of assembly process and control of involved robots. Petri nets are generally used for this modelling ([30], [31], [32]).
The paper investigates modelling by Petri nets and control by dual visual servoing of the assembly of an advanced 3D device. The application is described (section II) and the corresponding motion modelling in (section III). Motion control based on both 2D visual servo (section IV) and 3D visual servo (section V) is presented and the results obtained are presented and discussed (section VI).

II. Application

The application studied is the assembly of five parts by their U-grooves to get stable 3D structures, without any use of soldering effect (figure 1). The parts and their grooves measure 400 μm $\times$ 400 μm $\times$ 100 μm $\pm$ 1.5 μm and 100 μm $\times$ 100 μm $\times$ 100 μm $\pm$ 1.5 μm leading to an assembly clearance ranging from -3 and +3 μm. It is a test device that highlights most of the problems of 3D assembly, notably the need of precision in the control of robot dedicated to the application.
The setup used is positioned inside a controlled environment

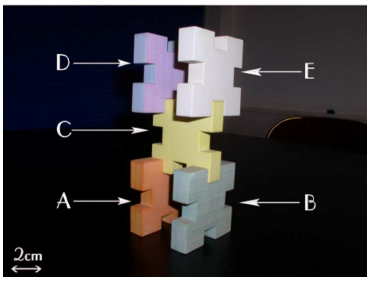

Fig. 1. Target 3D device at macroscale

on a vibration-free table (figure 2, table II). It comprises a 5 degree-of-freedom robotic systems distributed into two robots: a xyα robot and a zφ robot. The former robot (positioning table) is equipped with a compliant support and enables positioning of parts in horizontal plane while the latter robot (manipulator) supports the gripper and enables vertical positioning and spatial orientation of parts. A 2-finger gripper with 4 degree-of-freedom (2 per finger) as described in ([33]) is used as handling system. Two optical microscopes positioned vertically (Leica MZ 16 A) and laterally at 45 (140 mm Navitar tube) enable visual feedback of the workfield. According to the references [34], [35], [36] and [37] both may be described by the linear perspective model whose parameters may be determined using a 2D calibration rig.

III. Motion modelling by Petri nets

Modelling will meet the following policies:

- a task will be associated with a transition (possibly timed, represented by a rectangle),
- a state will be associated with a place (possibly with tokens, represented by a circle).

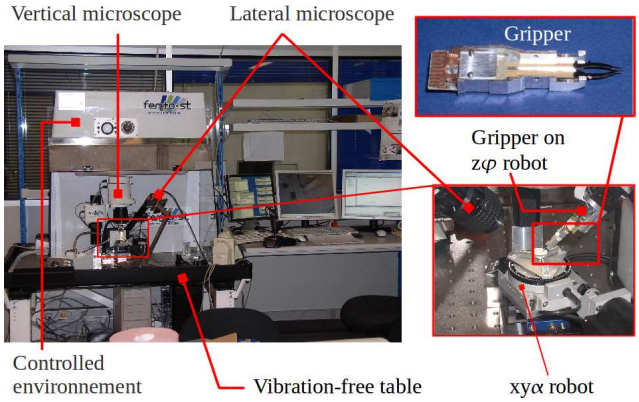

Fig. 2. Assembly setup

device	specifications
robot	linear/angular resolution: 0.05μm / 26μrad
gripper	horizontal/vertical stroke: 320μm / 200μm
vertical microscope	magnification/depth-of-field: 0-11× / 3 mm - 0.035 mm
lateral microscope	magnification/depth-of-field: 0-7× / 1 mm - 0.1 mm

TABLE I
SPECIFICATIONS OF THE SETUP

The application considered is nothing but the generalization of the assembly of two parts, **A** and **B** for example. The problem consists in the positioning of **A** followed by the positioning of **B** into the vertical groove of **A**. Since initially all parts are positioned on the table, only the motions of **B** involve the gripper. Then, the assembly process may be described by the Petri net of figure 3.

Positioning of **A** is a single task of displacement: displacement of **A** from its initial position to its final position by means of xyα table. In comparison, positioning of **B** is more complicated, it includes several tasks: gripping of **B**, displacement of **B** to the insertion site (pre-insertion displacement of **B**), displacement of **B** to final site (insertion displacement of **B**), release of **B**. The corresponding model is represented figure 4.

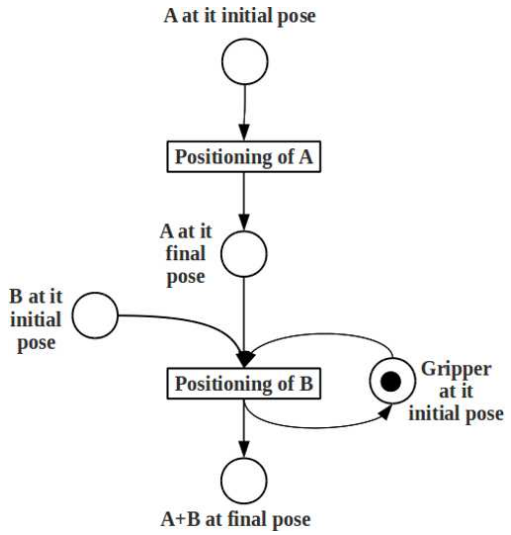

Fig. 3. Petri net modelling assembly process of parts **A** and **B**.

Control of these tasks are strongly dependant on imaging system available and visual servoing used, the better these elements the better the performing. The following configurations are used for their relevances with respect to the problem: (vertical microscope, 2D visual servoing) for gripping and release tasks and (lateral microscope, 3D visual servoing) for displacement tasks. An interesting point of the setup is that the vertical microscope is fully controllable by computer (focus, magnification and acquisition) leading to the opportunity to overcome the limitation of the depth-of-field by performing a dynamic autofocus of the microscope. It also enable the performing of coarse to fine 2D visual servo by introducing the magnification γ in the control law (multiscale visual servo).

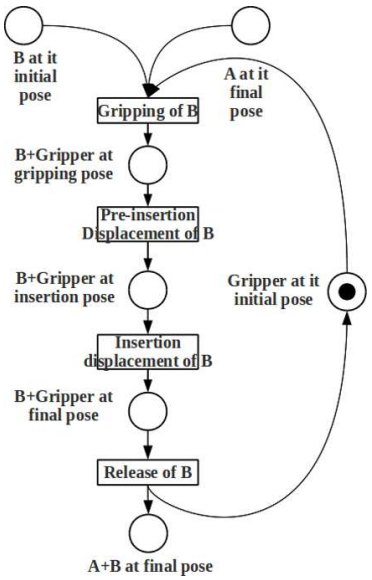

Fig. 4. Petri net modelling positioning of **B**.

IV. GRIPPING USING MULTISCALE 2D VISUAL SERVO

Gripping of **B** includes the following tasks: zooming in, autofocusing, **B** detection, opening of the gripper fingers, part aligning and centering with respect to the gripper fingers, descent of the gripper down to the gripping plane, closing of the gripper to grip the part, zooming out, ascent of the gripper with the part (figure 5). Four systems are controlled in this task: gripper (opening, closing), $z\varphi$ robot (descent, ascent), microscope (zooming in, zooming out, autofocusing), $xy\alpha$ robot (aligning and centering).

Let $P_i, i = 1, 2, 3, 4$ be the four points delimiting the bonding box of a part. The tracking of these points are performed by the robust approach described in [38] and [39] which gives every time t and magnification γ the poses of the points in the image frame $(u_i, v_i)^\top$ that may be normalized using calibration parameters to $s_i = (x_i, y_i)^\top$:

$$x_i = \frac{u_i - c_u}{f(\gamma)}, \qquad y_i = \frac{v_i - c_v}{f(\gamma)} \tag{1}$$

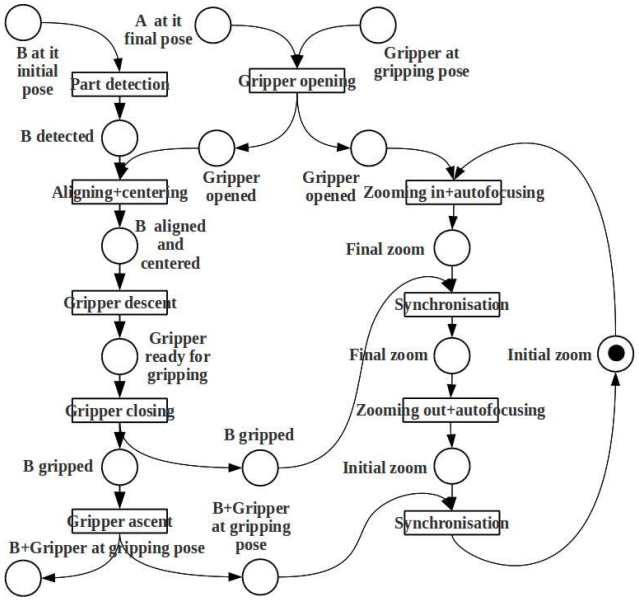

Fig. 5. Sequence of basic tasks corresponding to gripping

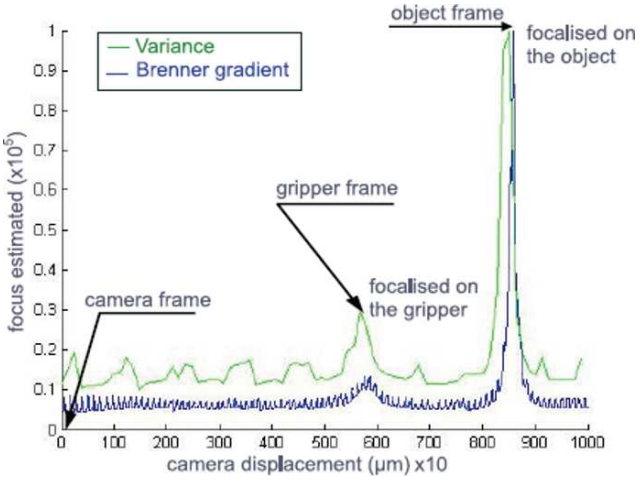

Fig. 6. Depth estimation from focus analysis

with $(c_u, c_v)^\top$) and $f(\gamma)$ the coordinates of the principal point and the focal length respectively.
Let s be the concatenation of the poses of the four points:$s = (s_1, s_2, s_3, s_4)^\top$. Aligning and centering are performed by regulating to zero the error between the current "pose" s and the desired "pose" $s*$ learned using a joystick (the part is under the gripper) that leads to the following control law (based on exponential decrease) of the $xy\alpha$ robot:

$$\begin{pmatrix} v_x \\ v_y \\ \omega_\alpha \end{pmatrix} = -\lambda L^+(Z*, \gamma)(s - s*) \tag{2}$$

with $L^+(Z*, \gamma)$ the pseudo inverse of the interaction matrix $L(Z*, \gamma)$ defined by $L(Z*, \gamma) = (L_1(Z*, \gamma), L_2(Z*, \gamma), L_3(Z*, \gamma), L_4(Z*, \gamma))^\top$ where $L_i)$ is the interaction matrix of the point i as defined in [40]:

$$L_i(Z*, \gamma) = \begin{pmatrix} \frac{-1}{Z*} 0 \frac{x_i(\gamma)}{Z*} x_i(\gamma) y_i(\gamma) - (1 + x_i^2(\gamma)) y_i(\gamma) \\ 0 \frac{-1}{Z*} \frac{y_i(\gamma)}{Z*} (1 + y_i^2(\gamma)) - x_i(\gamma) y_i(\gamma) - x_i(\gamma) \end{pmatrix} \tag{3}$$

To improve the convergence rate and avoid overshot the gain changes with respect to the error as:

$$\lambda = \lambda_{min} + (\lambda_{max} - \lambda_{min}) e^{-\rho \|s - s*\|} \tag{4}$$

with λ_{min}, λ_{max} and ρ equal to 0.1, 1 and 40 respectively. The value of $Z*$ is estimated by using a depth-from-focus approach. At the beginning of the experiment the vertical microscope scans the scene along z-axis step by step. At every step an image is acquired and the focus is estimated using a variance focus estimator as described in **??**. The representation of focuses with respect to z gives 2 peaks, the lowest corresponds to the gripper (position Z_g) while the highest corresponds to the part frame (table, position Z_p):

$$Z* = |Z_p - Z_g| \tag{5}$$

(figure 6). Outside visual servo, the value of $Z*$ is used to control the $z\varphi$ robot for descent and ascent of the gripper:

$$z = Z* \tag{6}$$

The dynamic autofocus of the microscope is performed by synchronizing its motion with that of the $z\varphi$ robot.
Let e_1 and e_2 be the distance in pixel between the left finger and right finger of the gripper and the part respectively. Every finger is then closed using the following law:

$$u_{d1} = \frac{e_i}{N} \tag{7}$$

with N the number of iterations.
The tasks of release part **A** and **B** are performed using control approaches similar to above ones.

V. Displacement using 3D visual servo

The tasks to controlled are: displacement of **A**, pre-insertion displacement of **B** and insertion displacement of **B**.
Let R_F and R_c be the frame attached to the workfield and the camera (i.e. the videomicroscope), respectively. The tracking of **A** and **B** using the approach described in [41] gives every time their 3D poses in R_c that may be expressed in R_F using the homogeneous transformation matrix between both:

$$s_A = \begin{pmatrix} {}^F t_A \\ {}^F \mathbf{R}_A \theta u \end{pmatrix} \tag{8}$$

$$s_B = \begin{pmatrix} {}^F t_B \\ {}^F \mathbf{R}_B \theta u \end{pmatrix} \tag{9}$$

${}^F t_i$ and $\mathbf{R}_i \theta u$ correspond to position and orientation of part i in the frame R_F.
Let s_{A*}, s_{B*} and s_{B**} be final pose of **A**, insertion pose of **B** and final pose of **B**. Suppose they are defined as:

$$s_A* = \begin{pmatrix} {}^F t_{A*} \\ 0 \end{pmatrix} \tag{10}$$

$$s_B* = \begin{pmatrix} {}^F t_{B*} \\ 0 \end{pmatrix} \tag{11}$$

$$s_B** = \begin{pmatrix} {}^F t_{B**} \\ 0 \end{pmatrix} \quad (12)$$

They are obtained by learning or directly from the CAD model.

Each task is performed by regulating to zero the error between current pose and desired pose.

Displacement of **A** involves the control the xyα table as:

$$\begin{pmatrix} v_x \\ v_y \\ \omega_\alpha \end{pmatrix}_F = -\lambda \begin{pmatrix} {}^F t_x - {}^F t_{x*} \\ {}^F t_y - {}^F t_{y*} \\ {}^F \mathbf{R}_A \theta u_\alpha \end{pmatrix} \quad (13)$$

Pre-insertion displacement of **B** involves the control of the xyα table as:

$$\begin{pmatrix} v_x \\ v_y \\ \omega_\alpha \end{pmatrix}_F = -\lambda \begin{pmatrix} {}^F t_x - {}^F t_{x*} \\ {}^F t_y - {}^F t_{y*} \\ {}^F \mathbf{R}_B \theta u_\alpha \end{pmatrix} \quad (14)$$

Insertion displacement of **B** involves the control of the zϕ manipulator as:

$$\begin{pmatrix} v_z \\ \omega_\phi \end{pmatrix}_F = -\lambda \begin{pmatrix} {}^F t_z - {}^F t_{z**} \\ {}^F \mathbf{R}_B \theta u_\varphi \end{pmatrix} \quad (15)$$

The gain λ is defined as described in equation 4.

VI. Results and Discussions

Figures 7 and 8 show some snapshots taken during the gripping. Evolution of gripping error is represented figures 9

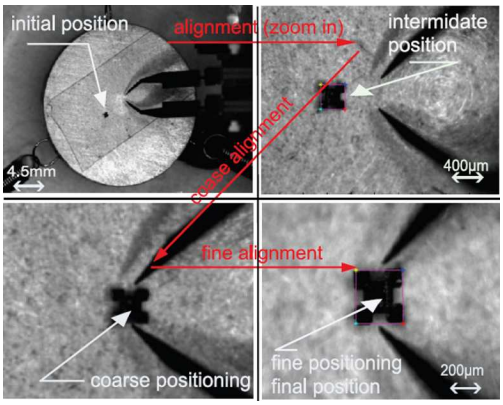

Fig. 7. Some shots of the workfield during the gripping: aligning, centering, zooming-in basic tasks

and 10 for the xyα robot: the final values are 2 μm and 7×10^{-3} radian for position and orientation respectively. Figure 11 shows some snapshots taken during the displacements. Evolution of displacement error is represented figures 12 and 13 for xyα robot and zφ robot respectively: the final values are 4 μm and 0.4×10^{-3} radian respectively. Precision of 2D visual servo is better than that of 3D visual servo, in accordance with theory: 2 μm against 4 μm.

Figure 14 shows some SEM (scanning electron microscope) images of the final assembly. The obtained mechanical play is about 3μm showing the relevance of tracking to deliver high quality pose measurement and control to compute precise laws, compatible with microassembly requirements. The assembly is performed many times: the success and

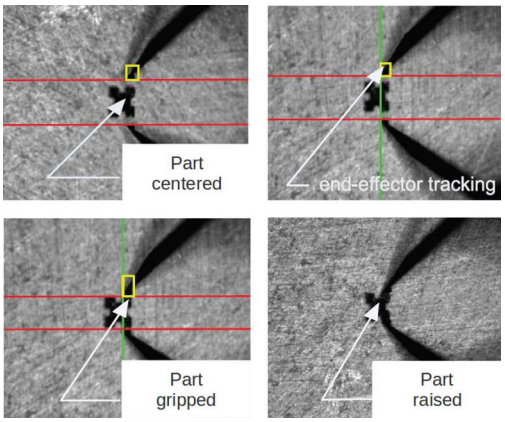

Fig. 8. Some shots of the workfield during part gripping: final result

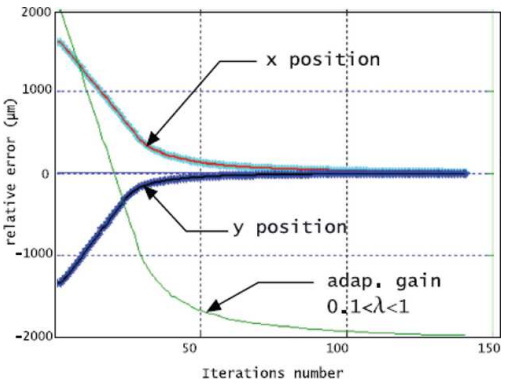

Fig. 9. Evolution of gripping error: position

failure ratios are 72 % and 28% respectively, the cycle time is about 40 s. These performances show the relevance of visual servo approaches to 3D microassembly and allow to consider their application to industrial cases. The sources of failure are:

- 17% for occlusions: occlusions of part by gripper cause the failure of part tracking,
- 22% for control error: controls are not precise enough to avoid the failure of tasks,
- 24% for capillary force: hydrometry of the scene is high enough to prevent release of part,

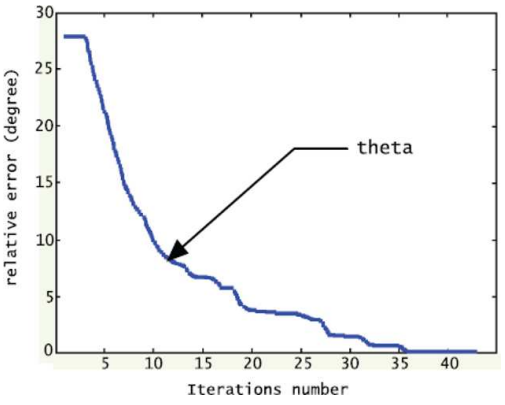

Fig. 10. Evolution of gripping error: orientation

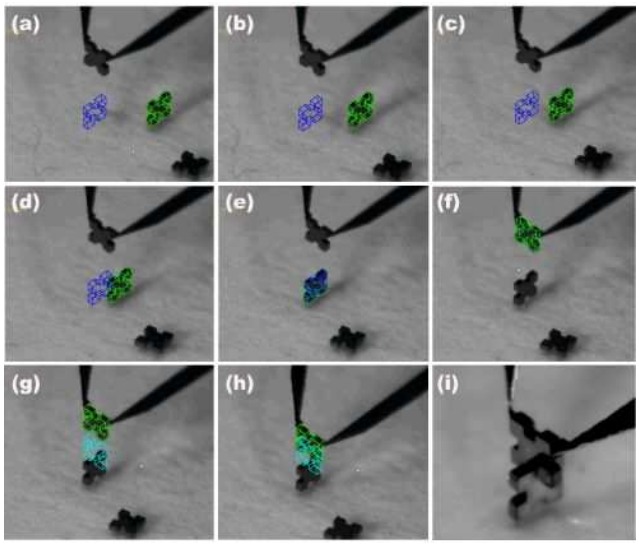

Fig. 11. Some shots of workfield during part displacements

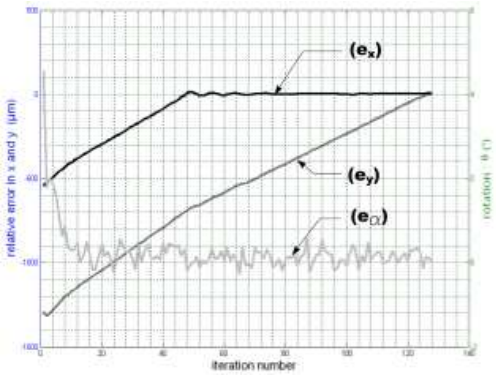

Fig. 12. Evolution of displacement error: xyα robot

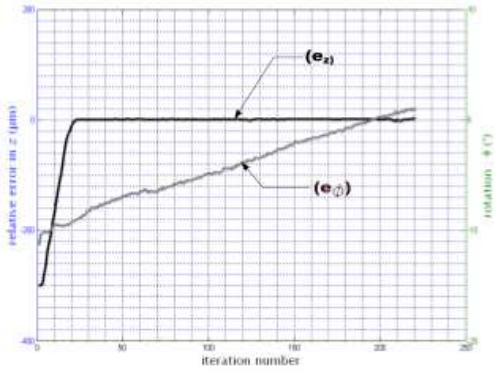

Fig. 13. Evolution of displacement error: zφ robot

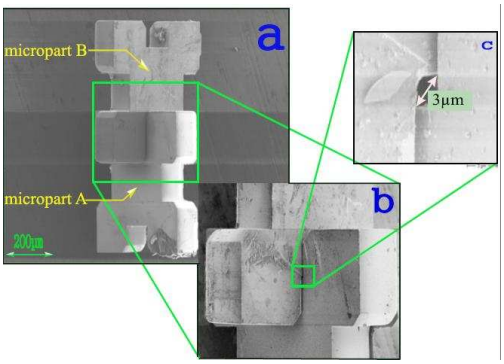

Fig. 14. Some images of the assembled structure from a scanning electron microscope

- 37% for electrostatic force: presence of electric charges on both parts and fingers cause the formers to move so uncontrolled.

Improvement of the success rate requires reduction of electrostatic and capillary forces, that may be obtained by efficient control of environment and functionalization of gripper fingers. Figure 15 shows some images of the final assembly of 5 parts and some steps: a right and stable structure is obtained without any use of soldering effect.

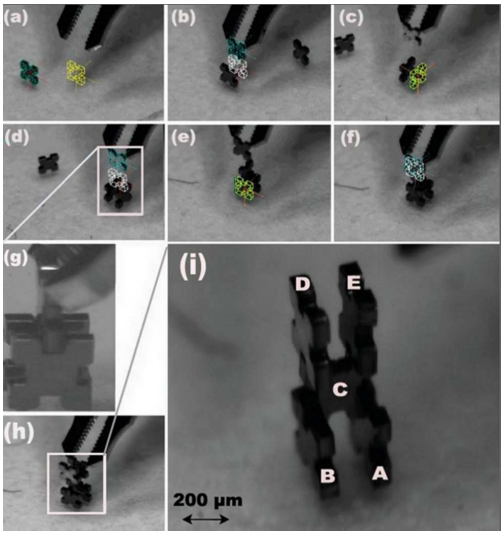

Fig. 15. Assembly of five parts on three levels.

REFERENCES

[1] Kanna Aoki, Hideki T. Miyazaki, Hideki Hirayama, Kyoji Inoshita, Toshikiko Baba, Kazuaki Sakoda, Norio Shinya, and Yoshinobu Aoyagi. Microassembly of semiconductor three-dimensional photonic crystals. *Nature Materials*, 2(2):117–121, 2003.

[2] S Rosen, HT Schmidt, P Reinhed, D Fischer, RD Thomas, H Cederquist, L Liljeby, L Bagge, S Leontein, and M Blom. Operating a triple stack microchannel plate-phosphor assembly for single particle counting in the 12-300 k temperature range. *Review of scientific instruments*, 78:13301–13301, 2007.

[3] Benjamin Gesemann, Stefan L. Schweizer, and Ralf B. Wehrspohn. Thermal emission properties of 2d and 3d silicon photonic crystals. *Photonics and Nanostructures - Fundamentals and Applications*, 8:107–111, 2010.

[4] Chris J. Brooks, Andrew P. Knights, and Paul E. Jessop. Vertically-integrated multimode interferometer coupler for 3d photonic circuits in soi. *Optics Express*, 19:2916–2921, 2011.

[5] V Crnojevic-Bengin and D Budimir. Novel 3d hilbert microstrip resonators. *Microwave and optical technology letters*, 46:195–197, 2005.

[6] Bruno Bêche, Arnaud Potel, Jérémy Barbe, Véronique Vié, Joseph Zyss, Christian Godet, Nolwenn Huby, David Pluchon, and Etienne Gaviot. Resonant coupling into hybrid 3d micro-resonator devices on organic/biomolecular film/glass photonic structures. *Optics Communications*, 283:164–168, 2010.

[7] PG Emma and E Kursun. Is 3d chip technology the next growth engine for performance improvement? *IBM journal of research and development*, 52:541–552, 2008.

[8] J.U. Knickerbocker. 3d chip technology preface. *IBM journal of research and development*, 52:539–540, 2008.

[9] L. Cadix, C. Bermond, C. Fuchs, A. Farcy, P. Leduc, L. DiCioccio, M. Assous, M. Rousseau, F. Lorut, L.L. Chapelon, B. Flechet, N. Sillon, and P. Ancey. Rf characterization and modelling of high density through silicon vias for 3d chip stacking. *Microelectronic Engineering*, 87:491–495, 2010.

[10] K Sakuma, S Kohara, K Sueoka, Y Orii, M Kawakami, K Asai, Y Hirayama, and JU Knickerbocker. Development of vacuum underfill technology for a 3d chip stack. *Journal of Micromechatronics and Microengineering*, 21:35024–35024, 2011.

[11] Niklas Frische, Proyag Datta, and Jost Goettert. Development of a biological detection platform utilizing a modular microfluidic stack. *Microsystems Technology*, 16:1553–1561, 2010.

[12] Kamil S. Salloum and Jonathan D. Posner. A membraneless microfluidic fuel cell stack. *Journal of Power Sources*, 196:1229–1234, 2011.

[13] Bradley J. Nelson, Steve Ralis, Yu Zhou, and Barmeshwar Vikramaditya. *Force and vision feedback for robotic manipulation of the microworld*, volume 250/2000 of *Lecture Notes in Control and Information Sciences*, chapter Haptics In Experimental Robotics VI, pages 433–442. Springer Berlin, Heidelberg, 1999.

[14] Barmeshwar Vikramaditya and Bradley J. Nelson. Visually servoed micropositioning for robotic micromanipulation. *Microcomputer Applications*, 18:23–31, 1999.

[15] Yu Zhou, Bradley J. Nelson, and Barmeshwar Vikramaditya. Integrating optical force sensing with visual servoing for microassembly. *Journal of Intelligent and Robotic Systems*, 28:259–276, 2000.

[16] Stephen Ralis, Barmeshwar Vikramaditya, and Bradley J. Nelson. Micropositioning of a weakly calibrated microassembly system using coarse-to-fine visual servoing strategies. *IEEE Transactions on Electronics Packaging Manufacturing*, 23(2):123–131, 2000.

[17] Ge Yang, James A. Gaines, and Bradley J. Nelson. A surpervisory wafer-level 3d microassembly system for hybrid mems fabrication. *Journal of Intelligent and Robotic Systems*, 37(1):43–68, 2003.

[18] Dan O. Popa and Harry E. Stephanou. Micro and mesoscale robotic assembly. *Journal of Manufacturing Process*, 6(1):52–71, 2004.

[19] Ge Yang, James A. Gaines, and Bradley J. Nelson. Optomechatronic design of microassembly systems for manufacturing hybrid microsystems. *IEEE Transactions on Industrial Electronics*, 52(4):1013–1023, 2005.

[20] John T. Feddema and Ronald W. Simon. Visual servoing and cad-driven microassembly. *IEEE Robotics and Automation Magazine*, 5(4):18–24, 1998.

[21] Volkmar Eichhorn, Sergej Fatikow, Tim Wortmann, Christian Stolle, Christoph Edeler, Daniel Jasper, Ozlem Sardan, Peter Bggild, Guillaume Boetsch, Christophe Canales, and Reymond Clavel. Nanolab: A nanorobotic system for automated pick-and-place handling and characterization of cnts. In *2009 IEEE International Conference on Robotics and Automation*. AMIR Oldenburg, 2009.

[22] Daniel N. Pascual. Fabrication and assembly of 3d mems devices. *Solid State Technology*, 48(7):38–42, 2005.

[23] R. Saini, Z. Jandric, K. Tsui, T. Udeshi, and D. Tuggle. Manufacturable mems microcolumn. *Journal of Microelectronic Engineering*, 78-79:62–72, 2005.

[24] Arne Sieber, Pietro Valdastri, Keith Houston, Arianna Menciassi, and Paolo Dario. Flip chip microassembly of a silicon triaxial force sensor on flexible substrates. *Sensors and Actuators A*, 142(1):421–428, 2008.

[25] Hui Xie, Weibin Rong, and Lining Sun. A flexible experimental system for complex microassembly under microscale force and vision-based control. *International Journal of Optomechatronics*, 1(1):81–102, 2007.

[26] Martin Probst, Christoph Hrzeler, Ruedi Borer, and Bradley J. Nelson. A microassembly system for the flexible assembly of hybrid robotic mems devices. *International Journal of Optomechatronics*, 3(2):69–90, 2009.

[27] Brahim Tamadazte, Eric Marchand, Nadine Lefort-Piat, and Sounkalo Dembélé. Cad model based tracking and 3d visual-based control for mems microassembly. *International Journal of Robotics Research*, 29(11):1416–1434, 2010.

[28] Brahim Tamadazte, Nadine Lefort-Piat, and Sounkalo Dembélé. Robotic micromanipulation and microassembly using synchronized petri nets. *International Journal of Advanced Manufacturing Technology*, 26(4):420–426, 2005.

[31] M. Caccia, P. Coletta, G. Bruzzone, and G. Veruggio. Execution control of robotic tasks: a petri net-based approach. *Control Engineering Practice*, 13(8):959–971, 2005.

[32] René David and Hassane Alla. *Discrete, Continuous, and Hybrid Petri Nets*. Springer, 2010.

[33] J. Agnus, P. Nectoux, and N. Chaillet. Overview of microgrippers and design of a micromanipulation station based on mmoc microgripper. In *IEEE International Symposium on Computational Intelligence in Robotics and Automation, CIRA, Finland*, 2005.

[34] Yu Zhou and Bradley J. Nelson. Calibration of a parametric model of an optical microscope. *Optical Engeenering*, 38(12):1989–1995, 1999.

[35] Mehdi Ammi and Antoine Ferreira. Calibration of a microscope for a 3d telemicromanipulation system using a virtual pattern. In *7es Journées du pôle Microrobotique (3es journées du RTP Microrobotique), 7 et 8 décembre 2004, EPFL, Lausanne*, 2004.

[36] Michael Figl, Christopher Ede, Johann Hummel, Felix Wanschitz, Rolf Ewers, Helmar Bergmann, and Wolfgang Birkfellner. A fully automated calibration method for an optical see-through head-mounted operating microscope with variable zoom and focus. *IEEE TRANSACTIONS ON MEDICAL IMAGING*, Vol. 24, N 11:1492–1499, 2005.

[37] Brahim Tamadazte, Sounkalo Dembélé, and Nadine Le Fort-Piat. A multiscale calibration of a photon video microscope for visual servo control: Application to micromanipulation. In *ROSE 2008 - IEEE International Workshop on Robotic and Sensors Environments, Ottawa, Canada, 17-18 October*, 2008.

[38] Ezio Malis. Improving vision-based control using efficient second-order minimization techniques. In *Proceedings of IEEE International Conference on Robotics and Automation (ICRA 2004), May, 2004, New-Orleans, USA*, 2004.

[39] Geraldo Silveira and Ezio Malis. Real-time visual tracking under arbitrary illumination changes. In *Internation Conference on Computer Vision and Pattern Recognition (CVPR2007)*, 2007.

[40] François Chaumette and Seth Hutchinson. Visual servo control, part 1 : Basic approaches. *IEEE Robotics and Automation Magazine*, 13(1):82–90, 2006.

[41] Andrew I. Comport, Member, Eric Marchand, Muriel Pressigout, and François Chaumettemalis. Real-time markerless tracking for augmented reality: The virtual visual servoing framework. *IEEE Transactions on Visualization and Computer Graphics*, 12(4):615–628, 2006.